This is a repository copy of *Formation of a ternary oxide barrier layer and its role in switching characteristic of ZnO-based conductive bridge random access memory devices*.

Version: Published Version

Article:

APL Materials

Formation of a ternary oxide barrier layer and its role in switching characteristic of ZnO-based conductive bridge random access memory devices

Firman Mangasa Simanjuntak, Julianna Panidi, Fayzah Talbi, et al.

COLLECTIONS

Paper published as part of the special topic on Materials Challenges for Nonvolatile Memory

View Online   Export Citation   CrossMark

ARTICLES YOU MAY BE INTERESTED IN

Formation of a ternary oxide barrier layer and its role in switching characteristic of ZnO-based conductive bridge random access memory devices

View Online   Export Citation   CrossMark

Firman Mangasa Simanjuntak,[1,a)] (iD) Julianna Panidi,[1] (iD) Fayzah Talbi,[2] Adam Kerrigan,[2] (iD)
Vlado K. Lazarov,[2] (iD) and Themistoklis Prodromakis[1] (iD)

AFFILIATIONS

[1] Centre for Electronics Frontiers, University of Southampton, Southampton SO17 1BJ, United Kingdom
[2] Department of Physics, University of York, York YO10 5DD, United Kingdom

Note: This paper is part of the Special Topic on Materials Challenges for Nonvolatile Memory.
[a)]Author to whom correspondence should be addressed: f.m.simanjuntak@soton.ac.uk

ABSTRACT

The insertion of a metal layer between an active electrode and a switching layer leads to the formation of a ternary oxide at the interface. The properties of this self-formed oxide are found to be dependent on the Gibbs free energy of oxide formation of the metal (ΔG_f°). We investigated the role of various ternary oxides in the switching behavior of conductive bridge random access memory (CBRAM) devices. The ternary oxide acts as a barrier layer that can limit the mobility of metal cations in the cell, promoting stable switching. However, too low (higher negative value) ΔG_f° leads to severe trade-offs; the devices require high operation current and voltages to exhibit switching behavior and low memory window (on/off) ratio. We propose that choosing a metal layer having appropriate ΔG_f° is crucial in achieving reliable CBRAM devices.

Memristive technologies offer huge potential for future ultra-high density random access memory (RAM) applications.[1,2] The switching mechanism of the memristive device is based on the reduction–oxidation (redox) process within the metal/insulator (switching layer)/metal cell.[3,4] Based on the nature of the ions involved in the switching mechanism, memristive technologies can be classified into two classes: oxygen vacancy-RAM [OxRAM, also called valence change memory (VCM)][5] and conductive bridge-RAM [CBRAM, also called electrochemical metallization memory (ECM)].[6] OxRAM relies on the formation and rupture of an oxygen vacancy filament to control the flow of electrons from the cathode to the anode;[7] the oxygen vacancy defects are created by ionizing oxygen in the switching layer.[8,9] Meanwhile, CBRAM technology utilizes the ionization of metal electrode atoms (Ag, Cu, Ni, or Te cations) to create a conducting bridge.[8] The mobility of cations is higher than that of anions due to their smaller ionic size;

henceforth, CBRAM technology could offer a faster switching speed than OxRAM.[10]

The development of CBRAM, however, often suffers from switching instability. Many attempts have been made in order to control the diffusion and drift of the cation species in the switching layer and improve the switching stability. Some of the proposed methods are the employment of electrode nanoislands[11] and graphene templates,[12] utilization of a layer of nanorods,[13] surface oxidation[14] and irradiation,[15] electrode alloying,[16,17] and insertion of a metal layer below the active electrode.[18] The insertion of a metal layer is the most practical method since the other methods require complex fabrication flow and are time-consuming processes. Nevertheless, the insertion of a metal layer is always followed by the formation of interfacial oxide, and the implication of this newly formed oxide in the switching characteristics is still overlooked. This paper studied the impact of different metal insertion layers in

forming an oxide barrier layer and its implication to the resistive switching characteristics of CBRAM devices.

5×5 μm cross-point devices were fabricated using a lithography technique; the architecture of the sandwich devices is illustrated in Fig. 1. First, a 25 nm Pt bottom electrode (BE) was deposited on the SiO$_2$ substrate; a 50 nm Ti adhesion layer was deposited prior to the Pt deposition. Hereafter, a 60 nm ZnO switching layer was deposited from a ZnO target in Ar/O$_2$ mixed ambient employing sputtering technique (radio frequency mode, Angstrom Engineering, Inc.). The top electrode (TE) consists of Pt/Ag stack with a thickness of 10 and 30 nm, respectively. The Pt layer is used as a capping layer and to enhance the conductivity of the electrode. In order to study the effect of various barrier layer materials, a 3.5 nm Cr or Ti layer was inserted prior to the top electrode deposition. Devices without and with the Cr or Ti metal insertion layer were denoted as NoBL, CrBL, and TiBL, respectively. All metal deposition was carried out using an e-gun evaporator system (Lab 700, Leybold Optics GmbH). The electrical characteristic of the devices was investigated using the ArCOne system (ArC Instruments); the voltage sweep bias was employed to the TE, while BE was grounded. All devices used a current compliance (CC) during the positive voltage sweep to avoid device breakdown and −1.5 V for the negative voltage sweep. Element profile distribution and oxidation states of the layers were examined using x-ray photoelectron spectroscopy (XPS, Thetaprobe ThermoVG). Microscopy analysis was conducted using an atomic force microscope (AFM, Bruker Dimension Icon) and a transmission electron microscope (TEM, JEOL JEM-2100Plus).

Figure 2 shows the typical $I–V$ curves and endurance performance of the devices. The device made without a metal insertion layer (NoBL) can show reproducible switching employing CC as low as 10 μA. The NoBL device requires a voltage (Vform) of ~1.7 V to switch its pristine state to a low resistance state (LRS or on), called electroforming process. Hereafter, the devices exhibit a counterclockwise bipolar switching mode; the devices can be switched from the LRS to a high resistance state (HRS or off, reset process) using a negative voltage sweep and, hereafter, a positive sweep to switch the device back to an LRS (set process) [Fig. 2(a)]. The reset (Vreset) and set (Vset) voltages are found to be −0.83 and 0.34 V, respectively. The Vreset and Vset were calculated based on an

average of 100 switching cycles; a switching cycle represents a set and a reset process. The NoBL device demonstrates a high on/off ratio (four orders of magnitude) but poor endurance having high variation of HRS and many intermediate states during the consecutive 100 cycles [Fig. 2(b)]. Meanwhile, the devices made with an insertion metal layer require a higher CC to exhibit switching behavior, as depicted in Figs. 2(c) and 2(e). The CrBL device requires a CC as low as 100 μA to electroform the device and a Vform of ~1.5 V. Henceforward, the device can exhibit reset and set processes employing Vreset and Vset of −0.34 and 0.37 V, respectively. The device exhibits good endurance for more than 100 cycles with an on/off ratio of 42 times [Fig. 2(d)]. On the other hand, the TiBL device requires CC of 500 μA and a Vform of 2.4 V to have a complete forming. The device also needs a higher Vreset and Vset, which are −0.95 and 0.79 V, respectively. The TiBL device exhibits good endurance but with a much lower on/off ratio (six times) [Fig. 2(f)]. The statistical distribution of the three devices is shown in Fig. 2(g); the coefficient of variation [standard deviation (γ)/average (μ)][18] of the HRS significantly decreases after the insertion of the metal layer (γ/μ of NoBL, CrBL, and TiBL is 42.9%, 36.3%, and 10.5%, respectively), indicating a narrower distribution, and, indeed, enhances the switching stability. However, it is also followed by several trade-offs: the increase of the minimum switching current and the decrease of on/off ratio. Materials analysis was conducted to explain this phenomenon.

Depth-XPS analysis was conducted to elucidate the element profile distribution in the stack films, as depicted in Fig. 3(a). In the NoBL stack, Ag is slightly diffused into the top region of the ZnO [Fig. 3(a-i)]. Meanwhile, the insertion of the metal layer limits the Ag diffusion [Figs. 3(a-ii) and 3(a-iii)]. The profile also shows that the CrBL and TiBL stack regions consist of Cr, Zn, and O species, which could suggest the formation of CrZnOx and TiZnOx compounds, respectively. Note that high oxygen accumulation was observed in the CrBL and TiBL regions; this indicates that the formation of the ternary oxide compounds involves oxygen absorption from the ZnO layer. Henceforth, we investigated the oxidation state of Cr and Ti elements in corresponding regions to confirm the occurrence of the oxygen absorption mechanism. Figure 3(b) shows the XPS spectra of the Cr^{3p} core level in the CrBL stack. The spectra are fitted with a single peak centered at 43.6 eV; this indicates that Cr has a 3+
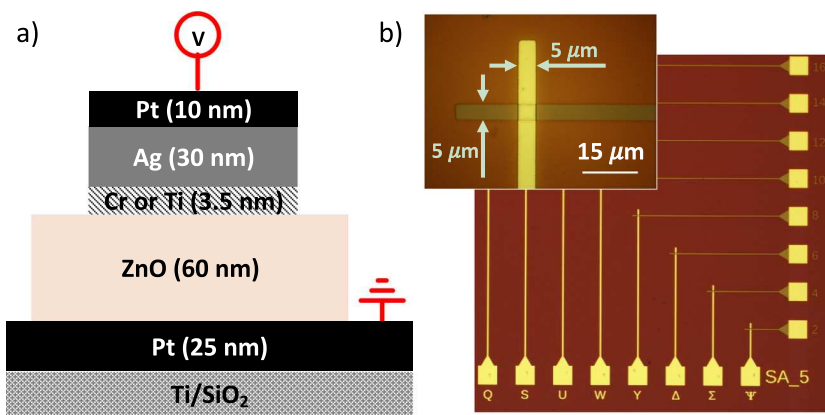

FIG. 1. (a) Schematic of the CBRAM device structure and electrical measurement setup. (b) Optical micrograph of the fabricated devices.
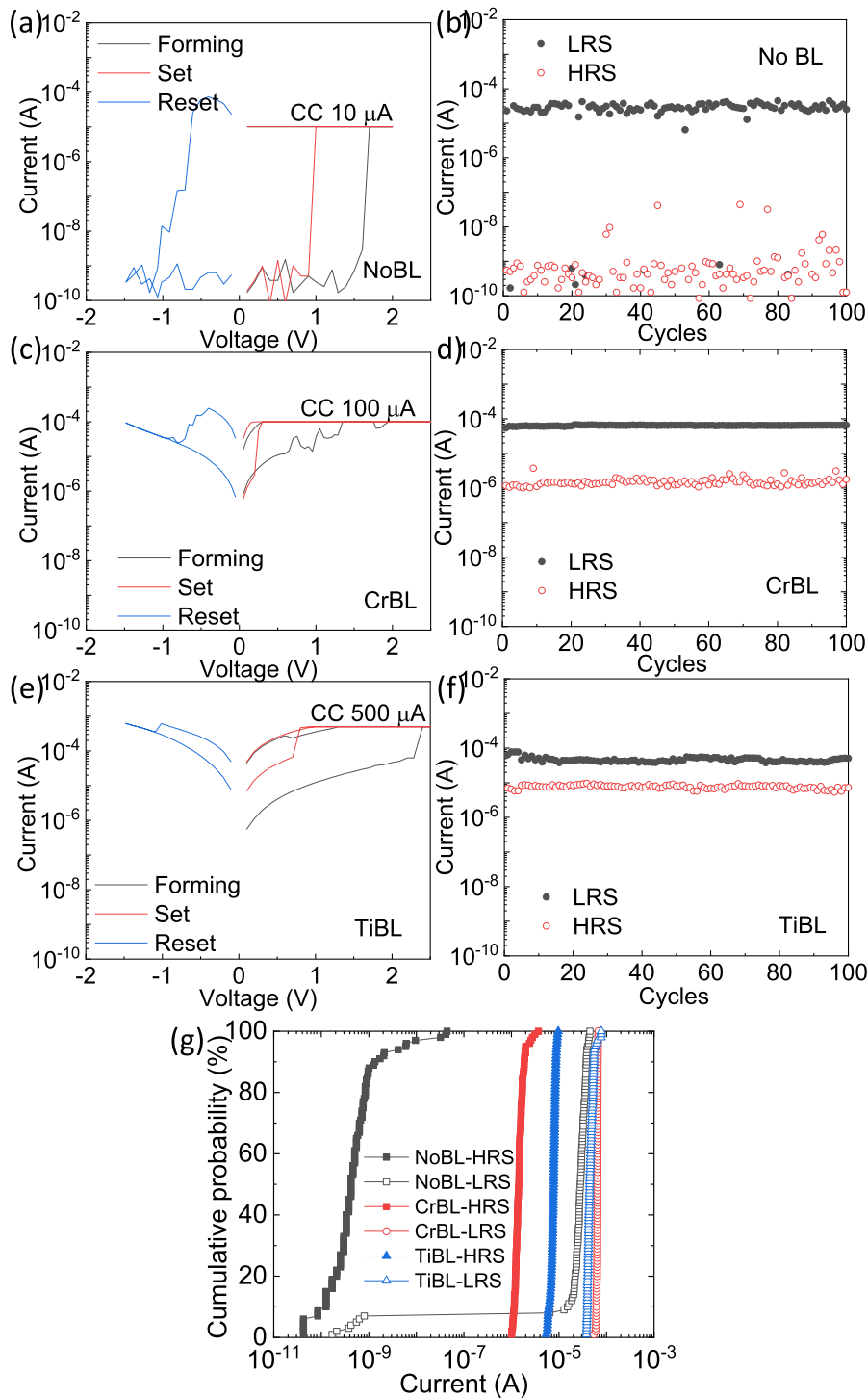
FIG. 2. Typical I–V curves and endurance performance of (a) and (b) NoBL; (c) and (d) CrBL; and (e) and (f) TiBL devices. A read voltage of −0.1 V was used to extract the LRS and HRS states. (g) Cumulative probability of the devices.

oxidation state.[19] Meanwhile, the XPS spectra of the Ti2p core level in the TiBL stack are fitted with multiple peaks centered at 457, 458.7 ($2p^{3/2}$), 460.3, 464.5 ($2p^{1/2}$), and 455.2 eV [Fig. 3(c)]; these imply the existence of multiple oxidation states (2+, 3+, and 4+).[20–22] The exhibition of a peak at the shoulder of the Ti2p$^{3/2}$ at lower

binding energy indicates the formation of a sub-oxide component.[23] This result confirms that both Cr and Ti are in an oxidized state, and they absorbed oxygen from the ZnO layer to form the interfacial compounds between the top electrode and the switching layer. We suggest that this is due to the lower (higher negative) Gibbs
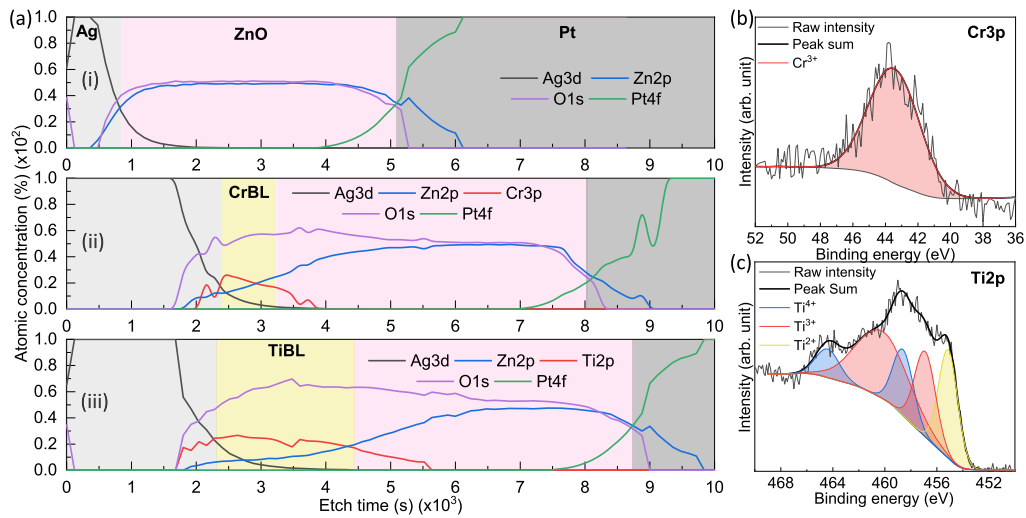
FIG. 3. (a) Depth-XPS element profile of the (i) NoBL, (ii) CrBL, and (iii) TiBL device stack structure. XPS spectra of (b) Cr3p and (b) Ti2p core levels.

free energy oxide formation of Cr and Ti than that of Zn [Cr_2O_3: -1058 kJ/mol, $TiOx$: $-2317 - (-1434)$ kJ/mol, ZnO: -320.5 kJ/mol].[24] Note that the TiBL has higher oxygen accumulation in the TiBL region, and the TiBL region is thicker as compared to the CrBL region. This is because the free energy formation of sub-oxide $TiOx$ is lower than that of Cr_2O_3.

AFM and TEM analyses were conducted to investigate the microscopic nature of the CrBL and TiBL regions, and the results
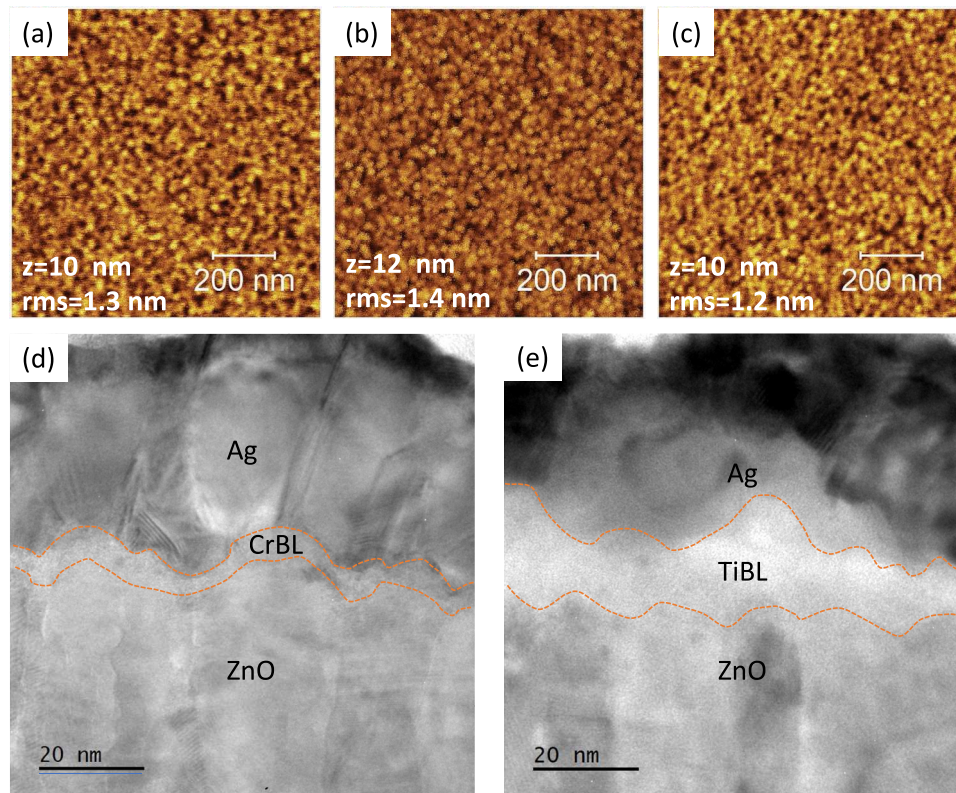

FIG. 4. AFM topography of (a) ZnO, (b) Cr, and (c) Ti deposited onto ZnO films, respectively. A cross-sectional TEM image of (d) Ag/Cr/ZnO/Pt and (e) Ag/Ti/ZnO/Pt devices.

are shown in Fig. 4. There is no significant surface roughness difference between the bare ZnO film [Fig. 4(a)] and after the barrier layer deposited onto it [Figs. 4(a) and 4(b)]. However, the cross-sectional TEM images show that the CrBL region is thinner than that of TiBL, as depicted in Figs. 4(d) and 4(e), respectively; the thickness of the CrBL and TiBL is ~4 and 9 nm, respectively, which confirms the XPS analysis. Note that both CrBL and TiBL show a continuous film on top of the ZnO grains and there is no indication on the formation of a nanoisland microstructure.

We propose a switching conduction mechanism to explain the electrical phenomenon, and the schematic is shown in Fig. 5. The ionization of Ag TE atoms initiates the formation of the conducting bridge in the CBRAM devices during a positive bias, and these Ag ions drift to the counter electrode to get oxidized back to Ag atoms.[25] These atoms create a bridge where the electrons can easily flow from the cathode to anode and switch the device to LRS (on).[25] The NoBL device has no barrier layer to control the Ag diffusion during the switching process [Fig. 5(a-i)]; hence, a high number of conducting bridges were formed during the electroforming process [Fig. 5(a-ii)]. These bridges can consist of one or few complete

bridge(s) and several incomplete bridges. During the reset process, most of the Ag atoms that make up the bridges can be ionized and drifted back to the top electrode and switch the device to HRS. Most of the bridges, if not all, can be ruptured during the reset process and leads to a large gap between top and bottom electrodes [Fig. 5(a-iii)] and, consequently, a high on/off ratio [Fig. 2(b)]. The rejuvenation of the bridge follows a similar fashion as the forming process; however, the structure of the bridge is different in each cycle [Fig. 5(a-iv)]. The location of the rupture and rejuvenation of the bridge is random. Thus, the bridge structure after reset and set processes can be varied, leading to the switching instability [Fig. 2(b)]. The insertion of a metal layer promotes the formation of a ternary oxide. This oxide acts as a barrier layer, limiting an excessive Ag drift during the formation and rupture of the bridge [Figs. 5(b) and 5(c)]. Since the ternary oxide absorbs oxygen from the ZnO layer [Figs. 3(b) and 3(c)], we can infer that the resistivity of the ZnO layer decreases. Note that ZnO has an abundance of intrinsic donor defects[26] and extraction of oxygen from this film will decrease its insulating behavior.[27] Henceforth, the pristine resistance state of CrBL and TiBL devices is lower than that of the NoBL device [Figs. 2(c) and 2(e)].
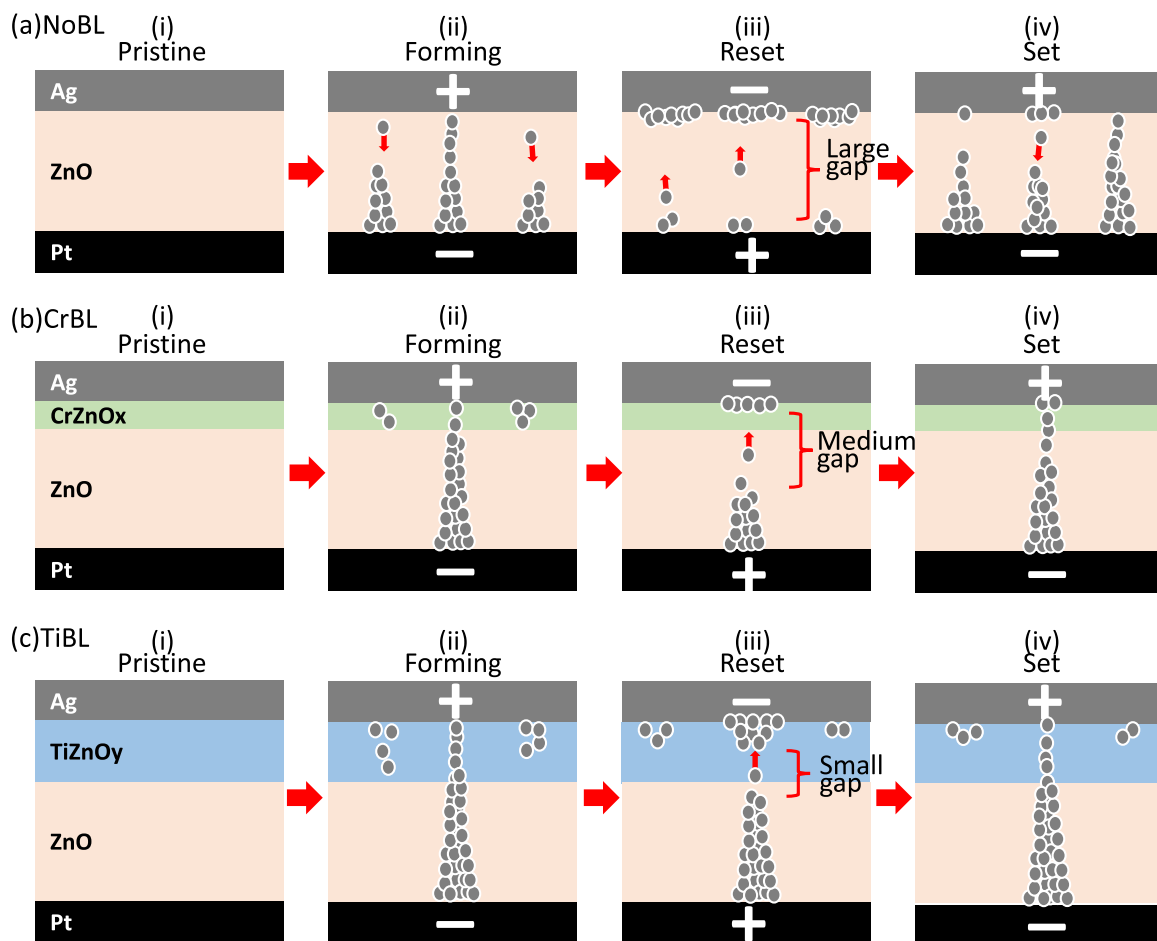

FIG. 5. Schematic of conduction mechanism during forming, reset, and set processes in (a) NoBL, (b) CrBL, and (c) TiBL devices.

The CrBL and TiBL devices require higher CC to exhibit switching behavior because a lesser insulating CBRAM cell needs a higher CC (or operating current) to complete the conducting bridge formation.[28] Both CrZnOx and TiZnOy barrier layers can limit Ag species involving in the switching process and avoid the occurrence of multiple bridge structures [Figs. 5(b-ii) and 5(c-ii)]. This indicates that the cations have lower mobility in these oxide regions, which could be due to a higher densely packed lattice than that of ZnO.[29] However, the thickness of the TiZnOy layer is excessively thick [Fig. 3(iii)], which further inhibits more Ag species drift back to the top electrode during the reset process and results in a small gap between the remnant bridge and the top electrode [low on/off ratio, Figs. 2(f) and 5(c-iii)]. We also suggest that the thick TiZnOx layer is responsible for the higher voltage operation (Vform, Vreset, and Vreset) in the TiBL device [Fig. 2(e)].

We studied the impact of various metal films for making a barrier layer in the CBRAM device structure. The device made without any metal insertion layer suffers from severe switching non-uniformity. On the other hand, the insertion of the Cr and Ti film below the Ag electrode leads to the formation of CrZnOx and TiZnOy ternary oxides, respectively, which act as a barrier layer to control the drift of Ag species during the switching process and induce stable switching. However, this enhancement is followed by several trade-offs: the requirement of higher current compliance and lower on/off ratio. The formation of these ternary oxides involves the absorption of oxygen from the ZnO oxide, and their thickness varies depending on their Gibbs free energy of oxide formation. Nevertheless, the CrZnOx barrier layer is found to be sufficient to avoid the formation of multiple bridge structures and good on/off ratio (~42 times) without the necessity of a high operation voltage and current (~0.3 V employing current compliance of 100 μA), which is beneficial to design the future low power data storage. This study emphasizes the importance of choosing a suitable metal insertion film to form a reliable barrier layer in designing reliable low-powered CBRAM devices.

AUTHOR DECLARATIONS

Conflict of Interest

The authors have no conflicts to disclose.

DATA AVAILABILITY

The data that support the findings of this study are available from the corresponding author upon reasonable request.

REFERENCES

[1] M. A. Zidan, J. P. Strachan, and W. D. Lu, Nat. Electron. **1**, 22 (2018).

[2] D. Panda, C.-A. Chu, A. Pradhan, S. Chandrasekharan, B. Pattanayak, S. M. Sze, and T.-Y. Tseng, Semicond. Sci. Technol. **36**, 045002 (2021).

[3] R. Waser and M. Aono, Nat. Mater. **6**, 833 (2007).

[4] D. Panda, P. P. Sahu, and T. Y. Tseng, Nanoscale Res. Lett. **13**, 8 (2018).

[5] F. M. Simanjuntak, S. Chandrasekaran, D. Panda, S. Rajasekaran, C. Rullyani, G. Madhaiyan, T. Prodromakis, and T.-Y. Tseng, Appl. Phys. Lett. **118**, 173502 (2021).

[6] M. Tada, T. Sakamoto, N. Banno, K. Okamoto, M. Miyamura, N. Iguchi, and H. Hada, in *2012 International Electron Devices Meeting* (IEEE, 2012), pp. 29.8.1–29.8.4.

[7] P.-Y. Jung, D. Panda, S. Chandrasekaran, S. Rajasekaran, and T.-Y. Tseng, IEEE J. Electron Devices Soc. **8**, 110 (2020).

[8] R. Waser, R. Dittmann, G. Staikov, and K. Szot, Adv. Mater. **21**, 2632 (2009).

[9] D. Panda and T.-Y. Tseng, Thin Solid Films **531**, 1 (2013).

[10] C. F. Chang, J. Y. Chen, C. W. Huang, C. H. Chiu, T. Y. Lin, P. H. Yeh, and W. W. Wu, Small **13**, 1–7 (2017).

[11] J. Wang, L. Li, H. Huyan, X. Pan, and S. S. Nonnenmann, Adv. Funct. Mater. **29**, 1808430 (2019).

[12] X. Zhao, S. Liu, J. Niu, L. Liao, Q. Liu, X. Xiao, H. Lv, S. Long, W. Banerjee, W. Li, S. Si, and M. Liu, Small **13**, 1603948 (2017).

[13] D. Panda, F. M. Simanjuntak, S. Chandrasekaran, B. Pattanayak, P. Singh, and T.-Y. Tseng, IEEE Trans. Nanotechnol. **19**, 764 (2020).

[14] F. M. Simanjuntak, S. Chandrasekaran, C.-C. Lin, and T.-Y. Tseng, Nanoscale Res. Lett. **13**, 327 (2018).

[15] F. M. Simanjuntak, T. Ohno, and S. Samukawa, ACS Appl. Electron. Mater. **1**, 18 (2019).

[16] Y. T. Tseng, I. C. Chen, T. C. Chang, J. C. Huang, C. C. Shih, H. X. Zheng, W. C. Chen, M. H. Wang, W. C. Huang, M. C. Chen, X. H. Ma, Y. Hao, and S. M. Sze, Appl. Phys. Lett. **113**, 053501 (2018).

[17] L. Qiao, Y. Sun, C. Song, S. Yin, Q. Wan, J. Liu, R. Wang, F. Zeng, and F. Pan, J. Phys. Chem. C **124**, 11438 (2020).

[18] S. Chandrasekaran, F. M. Simanjuntak, and T.-Y. Tseng, Jpn. J. Appl. Phys. **57**, 04FE10 (2018).

[19] M. Hassel, I. Hemmerich, H. Kuhlenbeck, and H.-J. Freund, Surf. Sci. Spectra **4**, 246 (1996).

[20] B. Bharti, S. Kumar, H.-N. Lee, and R. Kumar, Sci. Rep. **6**, 032355 (2016).

[21] R. H. Temperton, A. Gibson, and J. N. O'Shea, Phys. Chem. Chem. Phys. **21**, 1393 (2019).

[22] H. Tan, Z. Zhao, M. Niu, C. Mao, D. Cao, D. Cheng, P. Feng, and Z. Sun, Nanoscale **6**, 10216 (2014).

[23] R. L. Kurtz and V. E. Henrich, Surf. Sci. Spectra **5**, 179 (1998).

[24] J. A. Dean, *Lange's Handbook of Chemistry*, 15th ed. (McGraw-Hill, New York, 1999).

[25] I. Valov, R. Waser, J. R. Jameson, and M. N. Kozicki, Nanotechnology **22**, 254003 (2011).

[26] A. Janotti and C. G. Van de Walle, Phys. Rev. B **76**, 165202 (2007).

[27] A. Wang, T. Chen, S. Lu, Z. Wu, Y. Li, H. Chen, and Y. Wang, Nanoscale Res. Lett. **10**, 75 (2015).

[28] F. M. Simanjuntak, S. Chandrasekaran, B. Pattanayak, C.-C. Lin, and T.-Y. Tseng, Nanotechnology **28**, 38LT02 (2017).

[29] Y. Yang, P. Gao, S. Gaba, T. Chang, X. Pan, and W. Lu, Nat. Commun. **3**, 732 (2012).